Quaternary Science Reviews 169 (2017) 99–113

Contents lists available at ScienceDirect

Quaternary Science Reviews

journal homepage: www.elsevier.com/locate/quascirev

(MIS3 & 2) millennial oscillations in Greenland dust and Eurasian aeolian records – A paleosol perspective

Denis-Didier Rousseau [a, b, *], Niklas Boers [a], Adriana Sima [a], Anders Svensson [c], Matthias Bigler [d], France Lagroix [e], Samuel Taylor [e], Pierre Antoine [f]

[a] Ecole Normale Supérieure, UMR CNRS 8539, Laboratoire de Météorologie Dynamique, and CERES-ERTI, 24 rue Lhomond, 75231 Paris Cedex 5, France
[b] Lamont-Doherty Earth Observatory of Columbia University, Palisades, NY 10964, USA
[c] Centre for Ice and Climate Niels Bohr Institute, University of Copenhagen, Juliane Maries Vej 30, DK-2100 Copenhagen OE, Denmark
[d] University of Bern, Physics Institute, Climate and Environment Physics, Sidlerstrasse 5, CH-3012 Bern, Switzerland
[e] Institut de Physique du Globe, UMR CNRS 7154, 1 rue Jussieu, 75005, Paris, France
[f] CNRS, Laboratoire de Géographie Physique: Environnements Quaternaires et Actuels, UMR CNRS 8591, 1 Place Aristide Briand, 92195 Meudon, France

ARTICLE INFO

Article history:
Received 6 October 2016
Received in revised form
9 May 2017
Accepted 15 May 2017

ABSTRACT

Since their discovery, the abrupt climate changes that punctuated the last glacial period (~110.6–14.62 ka) have attracted considerable attention. Originating in the North-Atlantic area, these abrupt changes have been recorded in ice, marine and terrestrial records all over the world, but especially in the Northern Hemisphere, with various environmental implications. Ice-core records of unprecedented temporal resolution from northern Greenland allow to specify the timing of these abrupt changes, which are associated with sudden temperature increases in Greenland over a few decades, very precisely. The continental records have, so far, been mainly interpreted in terms of temperature, precipitation or vegetation changes between the relatively warm "Greenland Interstadials" (GI) and the cooler "Greenland Stadials" (GS). Here we compare records from Greenland ice and northwestern European eolian deposits in order to establish a link between GI and the soil development in European mid-latitudes, as recorded in loess sequences. For the different types of observed paleosols, we use the correlation with the Greenland records to propose estimates of the maximum time lapses needed to achieve the different degrees of maturation and development. To identify these time lapses more precisely, we compare two independent ice-core records: $\delta^{18}O$ and dust concentration, indicating variations of atmospheric temperature and dustiness in the Greenland area, respectively. Our method slightly differs from the definition of a GI event duration applied in other studies, where the sharp end of the $\delta^{18}O$ decrease alone defines the end of a GI. We apply the same methodology to both records (i.e., the GIs are defined to last from the beginning of the abrupt $\delta^{18}O$ increase or dust concentration decrease until the time when $\delta^{18}O$ or dust recur to their initial value before the GI onset), determined both visually and algorithmically, and compare them to published estimates of GI timing and duration. The duration of the GI and consequently the maximum time for paleosol development varies between 200 and 4200 years when visually determined and between 200 and 4800 years when estimated algorithmically for GI 17 to 2, i.e. an interval running from 60 ka to 23 ka b2k (age before 2000 AD). Furthermore, we investigate the abruptness of the transition from stadial to interstadial conditions, which initiates the paleosol development. The average transition duration is 55.4 ± 16.1 (56.8 ± 19.6) years when determined visually, and 36.4 ± 13.4 (60.00 ± 21.2) years when determined algorithmically for the $\delta^{18}O$ (dust concentration). The $\delta^{18}O$ increases correspond to a mean temperature difference of 11.8 °C on the top of the Greenland ice sheet, associated with substantial reorganizations of the ecosystems in mid-latitude Europe.

1. Introduction

The last glacial period (110.6–14.6 ka) has been punctuated by strong and abrupt climate variations at millennial timescales, first

* Corresponding author. Ecole Normale Supérieure, UMR CNRS 8539, Laboratoire de Météorologie Dynamique, and CERES-ERTI, 24 rue Lhomond, 75231 Paris Cedex 5, France.
E-mail address: denis.rousseau@lmd.ens.fr (D.-D. Rousseau).

http://dx.doi.org/10.1016/j.quascirev.2017.05.020
0277-3791/

identified in Greenland (Dansgaard et al., 1993) and North Atlantic (Bond et al., 1992) records. In parallel, Europe has been strongly impacted by the North Atlantic millennial climate changes, as observed in different types of sediment records (Allen et al., 1999; Sanchez-Goni et al., 2000, 2002; Rousseau et al., 2002, 2007b; Genty et al., 2003; Müller et al., 2003; Boch et al., 2011). These North Atlantic changes are related to variations in the sea-ice extent and therefore also affected the moisture sources of precipitation on the Greenland ice sheet (Masson-Delmotte et al., 2005; Steen-Larsen et al., 2013). These variations in the extent of the sea ice during the last climatic cycle (Kutzbach and Guetter, 1986; Byrkjedal et al., 2006) impacted the westerlies and the position of the polar jet stream, and consequently storm track trajectories. Furthermore, the presence of ice sheets and ice caps over Great Britain, Scandinavia and the Alps enhanced the zonal circulation (Pausata et al., 2011), as recorded by the eolian deposits located along the 50°N latitude, and as supported by numerical experiments (Sima et al., 2009, 2013).

Eolian deposits from the European periglacial zone known as loess are mainly composed of well-sorted coarse silt particles (20–63 μm) aggregated by clay particles (Pecsi, 1990) that represent 5–15% of the total sediment. Fine but also coarse sands are present in variable amounts (1–30%) depending on the distance of the sedimentation area from the sources, subject to deflation. However, clay particles are mostly present in the palaeosols, resulting from the geochemical transformation (weathering) of the parent eolian material, in which they can reach up to 20–30% in the most developed soil horizons (Bt or Bw).

The grain-size range in the loess deposits is nevertheless much larger than the dust grain-size observed in the Greenland ice-cores due to differences in the mode and conditions of transport, as well as due to the distance to the main source(s) (Ruth et al., 2002; Fischer et al., 2007). Loess units correspond to particles transported at rather low elevations, in the active layer of the atmosphere (about 300 to maximum 3000 m) at regional to local scales (Rousseau et al., 2014), while dust deposited at high latitudes is transported at much higher elevations (Pye, 1987, 1995). Loess sequences are well-developed all over Europe, but especially in the so-called loess belt between 48° and 52°N (Fig. 1). Such intensive deposition of dust over Europe has been favored by the reduced arboreal cover even practically absent in NW Europe during both stadial and interstadial stages (Woillard, 1978; Fletcher et al., 2010), by the sea-level lowering, exposing large areas of the continental shelves to eolian erosion (Juvigné, 1985; Lautridou, 1985; Léger, 1990; Rousseau et al., 2007a, 2014; Sima et al., 2009, 2013), and by strong increases in fluvial transport and sedimentation by periglacial braided rivers (Lautridou et al., 1999; Antoine et al., 2007; Smalley et al., 2009). Extensive investigations of European loess series along a longitudinal transect at 50°N reveal that the millennial-scale climate variations observed in the North-Atlantic marine and Greenland ice-core records are preserved in loess sequences (Rousseau et al., 2007b, 2011) (Fig. 2, Supplementary Fig. 1). Among them, the Nussloch loess site, on the right bank of the Rhine valley, yields an important record of the last climatic cycle (Antoine et al., 2001, 2009). At this site, the sequence for the interval 45 ka to 18 ka is exceptionally detailed, and supported by an intensive dating effort combining AMS ^{14}C and luminescence methods (Hatté et al., 1999; Lang et al., 2003; Rousseau et al., 2007b; Tissoux et al., 2010; Moine et al., 2017). Alternating paleosol and loess units preserved in the last climate cycle record correspond to the interstadials (GI) and stadials (GS) described in the Greenland ice-cores, respectively (Dansgaard et al., 1993; Johnsen et al., 2001; Rousseau et al., 2002, 2007a, 2007b; Moine et al., 2008, 2017; Antoine et al., 2009). The nature of each of the paleosols observed in Nussloch was preliminarily related to the duration of the corresponding Greenland interstadials (Rousseau et al., 2007b) (Fig. 2), but also a higher concentration of terrestrial mollusks, which prefer cool and moist conditions (Moine et al., 2008). GI 8, for example, the longest interstadial during the 40 ka –15 ka period, is represented in the Nussloch stratigraphy by a well developed arctic brown soil, while the much shorter GI 3 and 2, among others, correspond to tundra gleys of variable thickness, or to weakly oxidized horizons marked, among other indicators, by a slightly increased total organic content (Rousseau et al., 2002, 2007b; Antoine et al., 2009) (Fig. 2). Recent rock magnetic investigations (Taylor et al., 2014) of the loess interval above the arctic

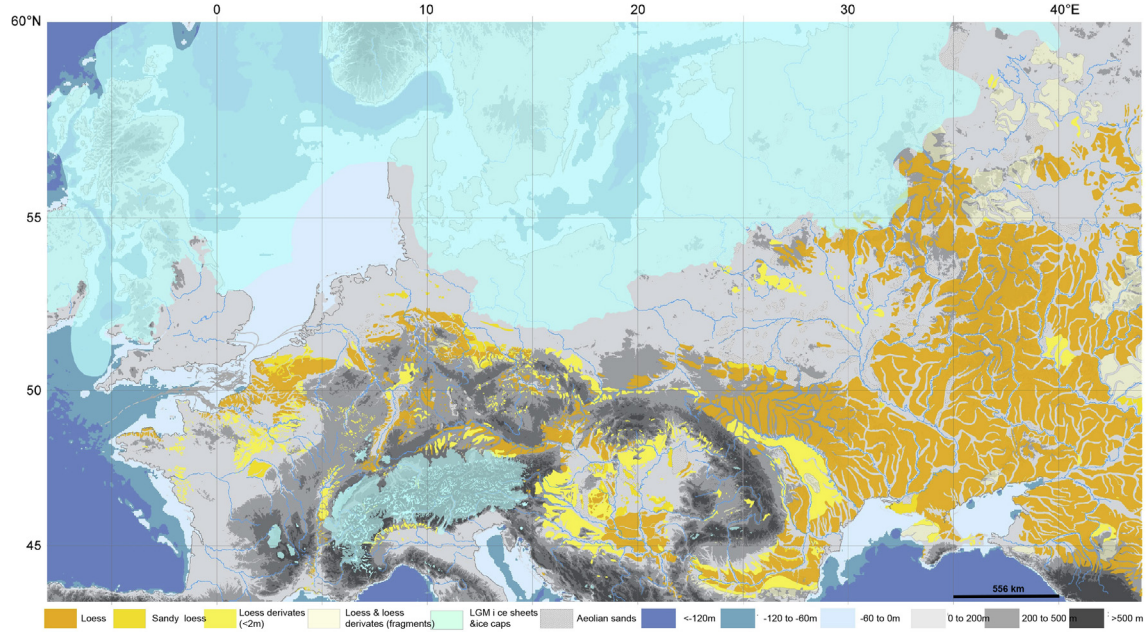

Fig. 1. Map of the main European loess deposits between –10° and 40° longitude and 60° and 45°N (after Antoine et al., 2013; Rousseau et al., 2014) with Last Glacial Maximum ice-sheets and ice caps extension.

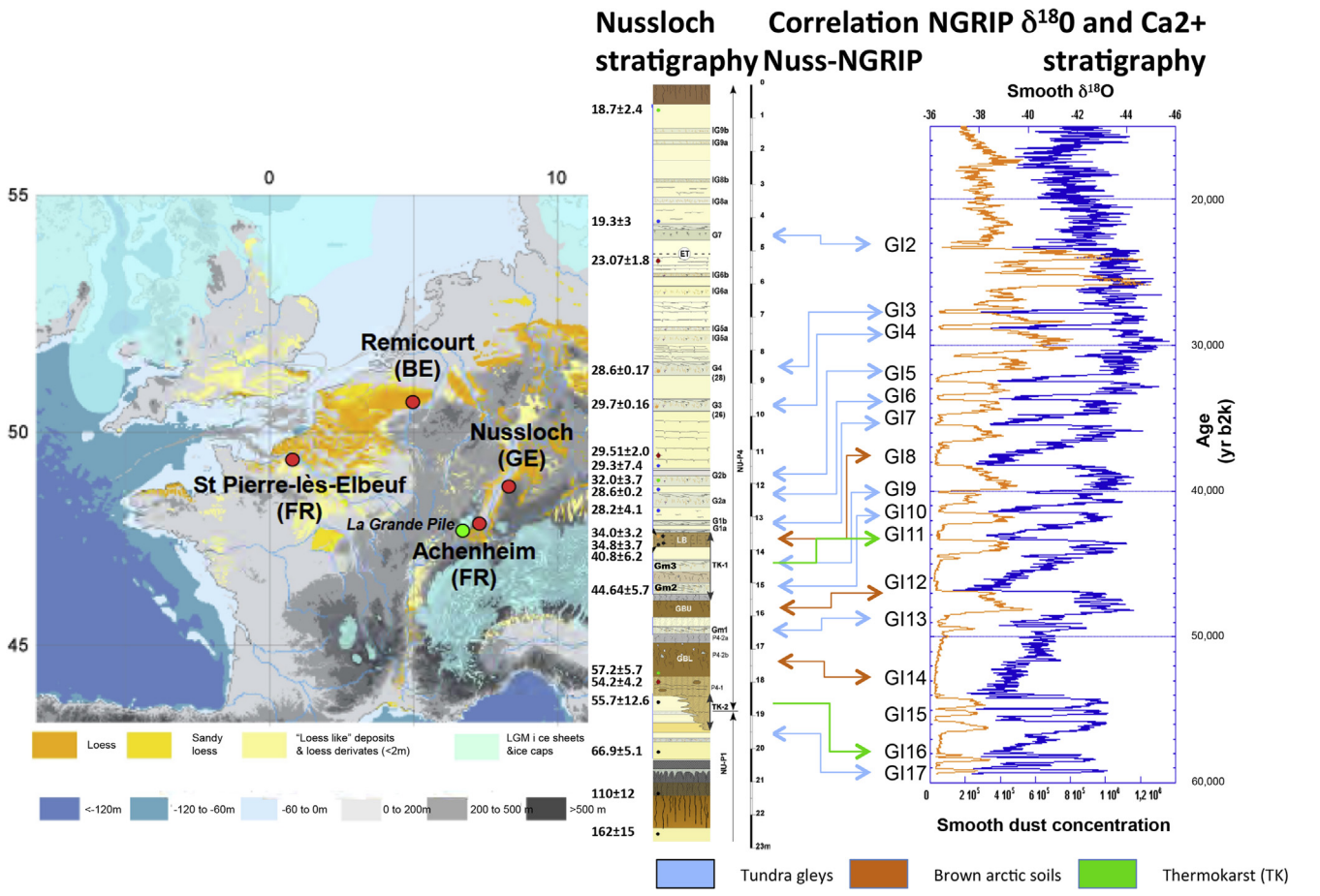

Fig. 2. Map of Western European loess deposits with location of the main sequences and the reference series from Nussloch. Stratigraphy of Nussloch last climate sequence, after Antoine et al. (2016) modified, showing the alternation of paleosols in brown and grey and eolian units in yellow. Correlation with the NGRIP $\delta^{18}O$ and dust record with assignment of the paleosol units to the Greenland interstadials (GI). The indicated dates are from Antoine et al. (2016) and Rousseau et al. (2007a,b). (The colors of the arrows refer to those applied in Fig. 7).

brown soil associated with GI 8 at Nussloch revealed bands of iron oxide dissolution associated with tundra gley units. Iron oxide dissolution and the possible iron re-precipitation leading to oxidized horizons correspond to a diagenetic alteration occurring at the base of the active layer, i.e. at the interface with permafrost, during limited warm and moist intervals. Such limited warming and increased moisture provide conditions favoring the transformation process (soil formation) in the tundra gley units, but the diagenetic alteration described above (dissolution) requires the presence of an impermeable layer, such as permafrost as postulated by Taylor et al. (2014) and references therein, to create an anoxic environment effectively dissolving the iron oxides. The subsequent re-precipitation of iron and the composition of this re-mineralisation will depend on local environmental and climate conditions. Taylor et al. (2014) observe, tentatively, a more important re-mineralisation in more developed tundra gley units that requires to be better quantified in future work but already supports the correlation with GIs of variable temporal duration (Fig. 2).

The Nussloch paleosol-loess unit couplet succession is not unique, but observed with a variable thickness and a diverse nature of the paleosols in sequences ranging from Western Europe eastward to Ukraine (Antoine et al., 2009, 2013; Rousseau et al., 2011), over more than 1800 km (Supplementary Fig. 1). The uncertainties concerning the duration of the soil formation are important because of the incompleteness of the paleosol profile, in particular for the interglacial soils in which the top horizons are often eroded. Nevertheless, arctic brown paleosols and tundra gleys do not show characteristics of erosion (Supplementary Fig. 2) on the outcrops. Furthermore the biological remains, mollusk shells (Moine et al., 2008) and earthworm granules (Prud'homme, 2017), characteristics of the upper levels of these paleosols, support such interpretation of lack of erosion. This therefore questions the definition of a correct time scale to be used for further model-data comparisons. In turn, this rises a problem in correctly estimating the mass accumulation rate (MAR) of the sequences for comparison with model estimates, which cannot be estimated by just taking into account the whole thickness of the considered deposits.

In the following section, we are refining the correlation between the paleosol succession observed in European loess sequences and the Greenland interstadials. In the third section we investigate the duration of the Greenland interstadials by studying high-resolution records of the $\delta^{18}O$ (NGRIP members, 2004; Gkinis et al., 2014) and dust concentration (Ruth et al., 2003) from the NGRIP record. This allows us to define the maximum duration of the development for the observed paleosols and discuss in the fourth section the low atmospheric dust load intervals in Greenland ice and their pedogenesis counterparts in Europe.

2. Refined assignment of European paleosols to Greenland interstadials

Paleosol formation is a complex process. Dates measured along a

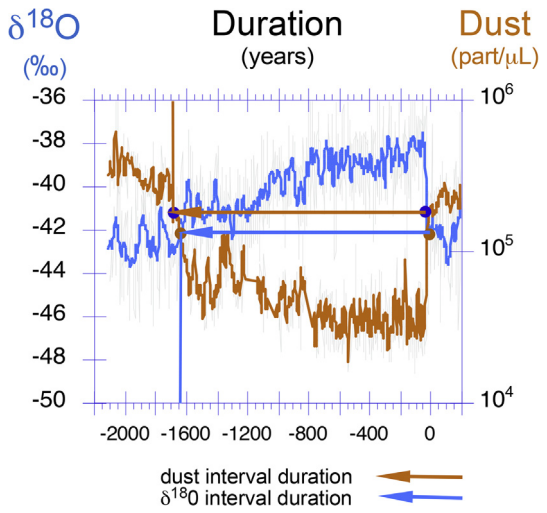

Fig. 3. Decomposition of Greenland interstadial $\delta^{18}O$ and dust concentration records from NGRIP ice core in relative time with zero placed at the start of the event. The start of the $\delta^{18}O$ increase is marked by the red dot and the start of the dust concentration decrease is marked by the blue dot around the zero year of the relative time scale. The end of the interstadial, determined as the return to the values at the start of the event, is also marked by a dot of the same color. The maximum duration of the event is the time lasting between the two dots and is indicated by the arrow in the figure. The transition time is the time between the start of the event and the interstadial value. (For interpretation of the references to colour in this figure legend, the reader is referred to the web version of this article.)

determined profile do not allow for a characterization of the type of pedogenesis, especially when considering the magnitude of their measured errors and the particular paleoenvironmental conditions of glacial times before and after the soil development. This makes the determination of the complete duration of the pedogenesis process a critical challenge. This is even more complicated when using different dating methods leading to diverse results. Indeed, some scientific dispute remains concerning the dating in our reference sequence of Nussloch, especially of the Lohner Boden paleosol assigned by Rousseau et al. (2002; 2007b) and Antoine et al. (2001, 2009) to GI 8, and thus an age of about 38.23–36.63 ka b2k is reported when referring to the NGRIP $\delta^{18}O$ timescale. This assignment is supported by luminescence dates from samples above this unit and one date of 40.2 ± 6.2 ka (Rousseau et al., 2007b) taken at the base of the Lohne Boden paleosol.

Kadereit et al. (2013) argued differently by indirectly assigning Lohne Boden to GI 7 by using ^{14}C dates from another unit not directly located in the stratigraphic succession. Interestingly, while our succession of paleosols, interpreted as climate events, fits with those observed in ice and marine cores (Rousseau et al., 2007b) (see correlations on Fig. 2), the opposed succession by Kadereit et al. (2013) implies more events than discussed in the literature or observed anywhere else, indicating that not every paleosol relates to a single interstadial/climate event. This is a main stratigraphic and climatic issue because of the location of the Nussloch series, which deposited through ridges-like on a plateau on the right edge of the Rhine valley. Such a geological and geographical context prevents any other interpretation than units observed in place, contrary to a depression, where additional local events like slumps, thermokarst infilling, or even missing units could have been recorded. Moreover, when we apply the same strategy downward the sequence prior to the Lohne Boden, two other brown paleosols (boreal brown soils) are observed in the lower part of the stratigraphy of the Nussloch Upper Pleistocene sequence, which have been correlated with the relatively long GI 12 and 14 (Rousseau et al., 2007b). Two different and independent luminescence dates of 57.2 ± 3.7 and 54.2 ± 4.2 (Bibus et al., 2007; Tissoux et al., 2010) support this assignment ($\delta^{18}O$ NGRIP age of GI 14: 54.23–50.03 ka b2k). The tundra gleys observed in between these two main brown arctic paleosols are assigned to shorter GI's and the number of gleys, similar to those of the GI, supports the rationale of the climate succession proposed by Rousseau et al. (2002, 2007b) for the upper part of the record (Fig. 2). We consider therefore that our assignment of GI 8 to the Lohner Boden is correct and that our published correlation between Nussloch loess sequence and NGRIP ice-core records remains accurate for our present study. Recent and new ^{14}C dates from earthworm granules from the identified paleosols in Nussloch finally support our initial interpretation and correlations (Moine et al., 2017).

A first estimate of the time interval of development of some paleosols in European sequences along 50°N was deduced by correlation with the GRIP ice-core dust record. For a given paleosol, this time interval was considered to start at the beginning of the abrupt decrease of dust concentration in the ice, associated with the corresponding rapid warming event, and to end when the dust concentration started to increase towards stadial values (Rousseau et al., 2011). Such rough estimates fitted with the duration of the pedological processes involved in building the different paleosols observed (Birkeland, 1984), but the temporal resolution of the Greenland ice-core record applied back then was very low. The estimate was therefore indicative, but nevertheless not realistic. Here we use high-resolution data from the NGRIP ice-core to estimate the duration of the intervals of relatively low atmospheric dust concentration for GI 17 to GI 2 (Section 3) much more precisely. These GIs have occurred between 60 ka to 23 ka b2k (Marine Isotope Stages MIS4, MIS3 and, partly MIS2), corresponding to the main interval of loess deposition in Europe, which ended at about 16–15 ka (Rousseau et al., 1998, 2007a). These interstadials are generally well-recorded in sequences from the European loess belt at around 50°N and in particular in our reference sequence of Nussloch. We interpret the episodes of low atmospheric dust load recorded in Greenland ice-cores as periods favorable to soil development in Europe with low to completely lacking dust emission and deposition (Sima et al., 2009, 2013). Thus, the GI duration is assigned to the corresponding paleosol types identified in European loess sequences as **maximum development duration** by considering the GI start and end (Section 3). We also discuss the abruptness of the transitions between stadial and interstadial conditions, when the soil formation begins (Section 4), and draw some conclusions (Section 5). Finally, pedostratigraphic and sedimentological analysis and dating clearly show that many of the short periods of climatic variations that Rasmussen et al. (2014) have identified in the Greenland interstadials have been too short events to be preserved as independent units in the continental record. As a consequence, this can result in the formation of polygenetic soil horizons, of soil complexes or even of very embryonic horizons as it is the case during the interval between (roughly) 60 and 35 ka (Moine et al., 2017).

3. Low dust concentration episodes in NGRIP ice core between 60 ka – 23 ka b2k

3.1. Characterization of NGRIP GI start and end (Figs. 3 and 4)

The dust and $\delta^{18}O$ data we use here are from the reference NGRIP ice core, to which the GICC05 multi-core multi-parameter layer-counted age scale is applied (Andersen et al., 2006; Rasmussen et al., 2006). For the time interval we address, 60 ka – 23 ka b2k, the layer counting has been performed using 7 parameters, taking into account the seasonal cycle (Andersen et al., 2006; Svensson et al., 2008). The layers considered by the

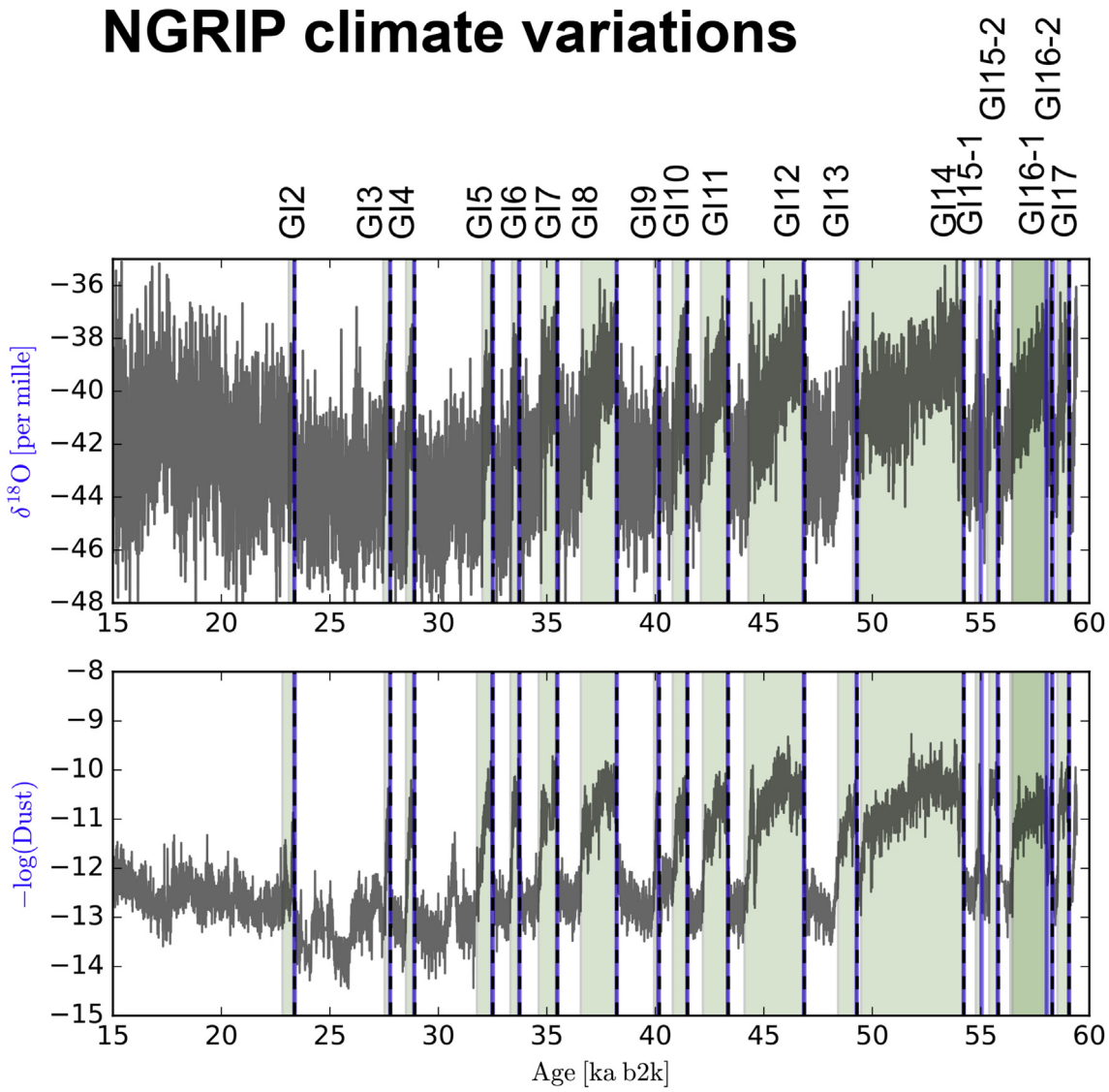

Fig. 4. NGRIP climate variations of the $\delta^{18}O$ and dust concentration records with the algorithmically detection of the Greenland interstadials (GI) from GI 2 to GI 17 (green shaded regions). (For interpretation of the references to colour in this figure legend, the reader is referred to the web version of this article.)

counting team as uncertain years were counted as 0.5 ± 0.5 years, and the cumulated uncertainty is treated as a Gaussian (2 sigma) error of the age scale. Wolff et al. (2010) summarize the ages of the GI warming events 17 to 2, determined by Andersen et al. (2006) and Svensson et al. (2008) from the $\delta^{18}O$ record, with the associated uncertainty. They also estimate the durations of GI 12 to 2, considered from the beginning of the abrupt $\delta^{18}O$ increase until the beginning of the sharp final drop. No duration was proposed for GI 17 to 13, whose complex structure did not allow these authors a clear identification of the end. Recently, Rasmussen et al. (2014) solved this problem and proposed a comprehensive definition of Greenland interstadials and stadials for the Last Glacial period by adopting the INTIMATE approach.

In this paper, we aim to correlate the duration of the GIs in the Greenland ice-core with the nature of the paleosols observed in our reference loess sequences. In order to do so, we need to estimate the duration of all the GIs in the studied interval, which is longer than that investigated by Wolff et al. (2010), but integrated within the whole Greenland ice-core record of the Last Glacial period from Rasmussen et al. (2014). We choose a slightly different method by separately analyzing two independent parameters of different origin, the dust and $\delta^{18}O$ records, and compare the results. To avoid the difficulties encountered by Wolff et al. (2010) for GI 17 to 13, we decided to proceed differently: the GI duration in the dust or $\delta^{18}O$ records is visually considered from the beginning of the initial sharp increase in $\delta^{18}O$ and sharp drop in dust concentration values until the time when the dust or $\delta^{18}O$ values return to their pre-transition values (Fig. 3). The justification of applying this method relies on the requirement of a stable environment, very low or no dust deposition), for a soil to develop. Considering the strong variability in both datasets and the aim of our study, the respective ages of the start of the abrupt transition, visually determined, are rounded to the nearest decade. (Table 1, columns *a,b*).

However, some objections could be proposed about the objectivity of the visual determination of the required interval boundaries observed in the NGRIP records. Therefore we developed the following algorithm to detect, differently and perhaps more robustly, the start and end dates of the stadial—interstadial transitions as well as the end dates of the interstadials (Fig. 4):

Table 1
Start and duration of GI 17 to 2 in the NGRIP dust and $\delta^{18}O$ records on the GICC05 timescale (in bold when the dust-derived value differs from the $\delta^{18}O$ one for a given GI).

GIS	[a]Start of abrupt transition in dust (yr b2k)	[b] Start of abrupt transition in ™^{18}O (yr b2k)	GI onset cf. references: *Andersen et al. (2006) **Svensson et al. (2008)			[e]Difference (b)-(c) (yr)	[f]GIS duration dust (100yr)	[g]GIS duration ™^{18}O (100yr)	[h]GIS duration Wolff et al. (2010) (100yr)	[i]Difference (g)-(h) (100yr)	[j]GIS duration Rasmussen et al. (2014) (100yr)	[k]Difference (g)-(j) (100yr)
			ref	[c]onset (yr b2k)	[d]1ó (yr))							
2	23 370	23 370	*	23 340	298	30	2	2	1	1	1	1
3	27 800	27 800	*	27 780	416	20	3	3	3	0	2	1
4	28 910	28 910	*	28 900	449	10	4	4	3	1	3	1
5	**32 500**	**32 520**	*	32 500	566	20	**6**	**5**	5	0	5	0
6	33 750	33 750	*	33 740	606	10	4	4	4	0	4	0
7	35 490	35 490	*	35 480	661	10	9	9	7	2	7	2
8	38 220	38 230	*	38 220	725	10	**17**	**16**	16	0	16	0
9	40 180	40 180	*	40 160	790	20	3	3	3	0	3	0
10	***41 490***	***41 480***	*	41 160	817	320	7	7	7	0	7	0
11	43 360	43 360	**	43 340	868	20	**12**	**11**	10	1	11	0
12	**46 870**	**46 890**	**	46 860	956	30	**27**	**26**	26	0	26	0
13	49 300	49 300	**	49 280	1015	20	**9**	**8**	n.d.		9	−1
14	**54 210**	**54 230**	**	54 220	1150	10	42	42	n.d.		46	−4
15	**55 810**	**55 830**	**	55 800	1196	30	4	4	n.d.		4	0
16	***58 290***	***58 280***	**	58 280	1256	0	**19**	**18**	n.d.		18	0
17	**59 070**	**59 080**	**	59 440	1287	−360	5	5	n.d.		9	−4

[a] Start of the GI initial abrupt transition in the dust record, visually determined on annual-resolution data and rounded to the nearest decade.
[b] Same as [a)] for the $\delta^{18}O$ record.
[c] GI onset visually determined as the midpoint of the initial abrupt increase in the 20-year averaged δ18O record by Andersen et al. (2006) for GI 10 to 2, and Svensson et al. (2008) for GI 17 to11.
[d] Counting uncertainty of the GICC timescale for the onset ages from [c)].
[e] Age difference between the GI start as defined in this study and the onset values cf. Andersen et al. (2006) and Svensson et al. (2008) and Rasmussen et al. (2014).
[f] GI duration in the dust record, rounded to the nearest century.
[g] Same as [f)] for the $\delta^{18}O$ record.
[h] GI duration estimated to the nearest century on $\delta^{18}O$ dataset by Wolff et al. (2010).
[i] Difference between the GI duration estimated here (g) and the Wolff et al. (2010) values (h).
[j] GI duration estimated to the nearest century on $\delta^{18}O$ dataset by Rasmussen et al. (2014).
[k] Difference between the GI duration estimated here (g) and the Rasmussen et al. (2014) values (j).

First, the $\delta^{18}O$ and dust records are interpolated to an equidistant time axis with 5 year-intervals.
Second, we defined an averaged derivative by computing for each time step the difference between the mean of the 30 subsequent time steps and the 30 previous time steps, both corresponding to 150 years. The local maxima of time periods for which this derivative is above the 95th percentile are then identified as approximate candidates for the GI transition dates. For each of the hereby-detected candidates (18 were detected contrary to the 16 that were detected visually), we look for the closest future maximum of the time series that is above the 70th percentile of the 30 subsequent time steps (i.e., 150 years). These maxima are identified as the end points of the respective transitions.
Third, we looked for the closest minima preceding the transition end points that are below the 60th percentile of the 30 time steps previous to the approximate GI transition date candidates. The 30 time steps preceding these minima are identified as pre-transition periods. We defined the start points of the transitions as the minima closest to (but preceding) the transition end points, such that they are below the 50th percentile of the pre-transition period.
Finally, the end dates of the interstadial periods are defined as the first time points following the transition end dates for which the 40 year running mean (10 year running mean) of the $\delta^{18}O$ (dust) time series falls below the 50th percentile of the respective pre-transition periods (Table 2).

3.1.1. GI start

The **GI start** ages of the abrupt transitions in the dust and $\delta^{18}O$ records, as estimated and rounded in this paper, are very close. For many of the analyzed GI, the difference is less than one decade. More notable are the GI 15, 14, 12 and 5, for which the transition in dust appears to start by about 2 decades later than in $\delta^{18}O$, and GI 16 and 10, for which the dust change begins about one decade earlier. These visual estimations are only indicative, and fit with the errors related to the dating methods used in the loess sections. We note that very detailed investigations of the same GI from the same ice core may not lead to exactly the same result. For example, the onset of GI 8 coincides in the NGRIP $\delta^{18}O$ and dust records in (Ruth et al. (2007)), while Thomas et al. (2009) find that the dust concentration decrease starts earlier than the $\delta^{18}O$ increase.

For comparison with our values, Table 1 (column *c*) also shows the GI onset ages visually determined at the midpoint of the initial abrupt increase in the 20-year averaged $\delta^{18}O$ record by Andersen et al. (2006) for GI 10 to 2, and Svensson et al. (2008) for GI 17 to 11. For 14 GIs out of the 16 analyzed, the differences between these estimations are less than 30 years, and mainly result from the fact that we consider the beginning instead of the midpoint of the transition. A quite special case is GI 16 and, in particular, how to define its onset. Indeed GI 16 could be considered as starting before or after the short event GI-16.2 observed at 58.2 ka b2k. Following the latter hypothesis, GI 16 shows a peculiar feature described earlier by Capron et al. (2010) for older intervals and named “precursors”. Precursors are described as short-lived abrupt warmings preceding interstadials. We decided to consider GI 16 as starting

Table 2
Start, end, duration of GI 17 to 2 and duration of the abrupt transitions between stadial and interstadial conditions in the NGRIP $\delta^{18}O$ and dust records on the GICC05 timescale.

GI	GI visually			GI algorithmcally			Differences visual vs algorithm			GI Rasmussen et al. (2014)			Differences in duration vs Rasmussen		GI transition			GI
	a)	b)	c)	d)	e)	f)	g)	h)	i)	j)	k)	l)	m)	n)	o)	p)	q)	
#	™18OstartVisual---rounded (yr b2k)	™18OendtVisual---rounded (yr b2k)	™18durationVisual---rounded (yr)	™18OstartAlgorithm---rounded (yr b2k)	™18OendtAlgorithm---rounded (yr b2k)	™18durationAlgorithm---rounded (yr)	Difference™18Ostart (yr)	Difference™18Oend (yr)	Difference™18Oduration (yr)	™18Ostart (yr b2k)	™18Oend (yr b2k)	duration (yr)	difference Visual---Rasmussen (yr)	difference Algorithm---Rasmussen (yr)	GI™18durationVisual (yr)	GI™18OdurationAlgorithm (yr)	GI™18OdurationVisual---Algorithm (yr)	#
2	23370	23180	200	23380	23110	270	---10	70	---70	23340	23220	120	80	150	53	30	---23	2
3	27800	27470	330	27790	27460	330	10	10	0	27780	27540	240	90	90	37	25	---12	3
4	28910	28510	400	28910	28510	400	0	0	0	28900	28600	300	100	100	34	35	1	4
5	32520	32030	500	32520	32030	500	0	0	0	32500	32040	460	40	40	59	30	---29	5
6	33750	33370	380	33740	33390	350	10	---20	30	33740	33360	380	0	---30	77	35	---42	6
7	35490	34640	850	35510	34730	780	---20	---90	70	35480	34740	740	110	40	60	65	5	7
8	38230	36600	1640	38240	36590	1650	---10	10	---10	38220	36580	1640	0	10	45	35	---10	8
9	40180	39870	320	40170	39940	230	10	---70	90	40160	39900	260	60	---30	59	10	---49	9
10	41480	40780	700	41480	40790	690	0	---10	10	41460	40800	660	40	30	56	40	---16	10
11	43360	42280	1090	43370	42100	1270	---10	180	---180	43340	42240	1100	---10	170	49	50	1	11
12	46890	44280	2610	46860	44290	2580	30	---10	30	46860	44280	2580	30	0	91	30	---61	12
13	49300	48470	840	49320	49110	210	---20	---640	630	49280	48340	940	---100	---730	54	55	1	13
14	54230	50030	4200	54240	49410	4830	---10	620	---630	54220	49600	4620	---420	210	54	50	---4	14
15.1				55010	54750	260				55000	54900	100		160		30		15.1
15.2	55830	55400	430	55820	55300	520	10	100	---90	55800	55400	400	30	120	80	50	---30	15.2
16.1				58050	56470	1590				58040	56500	1540		50		30	30	16.1
16.2	58280	56450	1830	58280	56440	1840	0	10	---10	58280	58160	120	1710	1720	42	35	---7	16.2
17.1	59080	58550	530	59080	58520	570	0	30	---40	59080	58560	520	10	50	36	20	---16	17.1
Mean			1053,13			1048,33	---0,63	11,88	---10,63			928,89	110,63	119,44	55,38	36,39	-	Mean
Std deviation			1068,43			1163,44	12,89	238,59	238,62			1128,46	444,23	447,15	16,12	13,37	22,22	Std deviation
Max			4200,00			4830,00	30,00	620,00	630,00			4620,00	1710,00	1720,00	91,00	65,00		Max
Min			200,00			210,00	---20,00	---640,00	---630,00			100,00	---420,00	---730,00	34,00	10,00		Min
	aa)	bb)	cc)	dd)	ee)	ff)	gg)	hh)	ii)	jj)	kk)	ll)	mm)	nn)	oo)	pp)	qq)	
#	duststartVisual---rounded (yr b2k)	dustendtVisual---rounded (yr b2k)	dustdurationVisual---rounded (yr)	duststartAlgorithm---rounded (yr b2k)	dustendtAlgorithm---rounded (yr b2k)	dustdurationAlgorithm---rounded (yr)	Differenceduststart (yr)	Differenceustend (yr)	Differenceustduration (yr)	duststart (yr b2k)	dustend (yr b2k)	duration (yr)	difference Visual---Rasmussen (yr)	difference Algorithm---Rasmussen (yr)	IGdustdurationVisual (yr)	IGdustdurationAlgorithm (yr)	IGdustdurationVisual---Algorithm (yr)	#
2	23370	23190	180	23430	22820	540	---60	370	---360	23340	23220	120	60	420	58	80	22	2
3	27800	27510	280	27800	27520	250	0	---10	30	27780	27540	240	40	10	40	25	---15	3
4	28910	28530	390	28940	28510	370	---30	20	20	28900	28600	300	90	70	30	65	35	4
5	32500	31860	640	32570	31780	680	---70	80	---40	32500	32040	460	180	220	59	115	56	5
6	33750	33310	430	33750	33320	390	0	---10	40	33740	33360	380	50	10	69	40	---29	6
7	35490	34620	870	35500	34620	830	---10	0	40	35480	34740	740	130	90	70	55	---15	7
8	38220	36540	1680	38260	36560	1640	---40	---20	40	38220	36580	1640	40	0	39	60	21	8
9	40180	39900	290	40190	39940	170	---10	---40	120	40160	39900	260	30	---90	109	80	---29	9
10	41490	40780	710	41490	40800	640	0	---20	70	41460	40800	660	50	---20	55	50	---5	10
11	43360	42200	1160	43370	42190	1120	---10	10	40	43340	42240	1100	60	20	38	55	17	11
12	46870	44190	2680	46910	44110	2720	---40	80	---40	46860	44280	2580	100	140	67	85	18	12
13	49300	48420	880	49310	48420	830	---10	0	50	49280	48340	940	---60	---110	57	55	---2	13
14	54210	50010	4200	54240	49480	4710	---30	530	---510	54220	49600	4620	---420	90	54	55	1	14
15.1				55050	54770	220				55000	54900	100		120		60		15.1
15.2	55810	55380	430	55790	55390	370	20	---10	60	55800	55400	400	30	---30	79	35	---44	15.2
16.1				58050	56470	1550				58040	56500	1540		10		35	35	16.1
16.2	58290	56380	1910	58310	56360	1890	---20	20	20	58280	58160	120	1790	1770	42	60	18	16.2
17.1	59070	58540	530	59110	58530	510	---40	10	20	59080	58560	520	10	---10	42	70	28	17.1
Mean			1078,75			1079,44	---21,88	63,13	---25,00			928,89	136,25	150,56	56,75	60,00	6,59	Mean
Std deviation			1078,95			1134,87	24,01	157,17	166,69			1128,46	459,84	421,98	19,61	21,21	26,92	Std deviation
Max			4200,00			4710,00	20,00	530,00	120,00			4620,00	1790,00	1770,00	109,00	115,00		Max
Min			180,00			170,00	---70,00	---40,00	---510,00			100,00	---420,00	---110,00	30,00	25,00		Min

a Start of the GI initial abrupt transition in the $\delta^{18}O$ record, visually determined on annual-resolution data and rounded to the nearest decade.
b End of the GI in the $\delta^{18}O$ record, visually determined on annual-resolution data and rounded to the nearest decade.
c Duration of the GI in the $\delta^{18}O$ record, visually determined on annual-resolution data and rounded to the nearest decade.
d Start of the GI initial abrupt transition in the $\delta^{18}O$ record, algorithmically determined on annual-resolution data and rounded to the nearest decade.
e End of the GI in the $\delta^{18}O$ record, algorithmically determined on annual-resolution data and rounded to the nearest decade.
f Duration of the GI in the $\delta^{18}O$ record, algorithmically determined on annual-resolution data and rounded to the nearest decade.
g Difference between visually and algorithmically determined start of the GI initial abrupt transition in the $\delta^{18}O$ record.
h Difference between visually and algorithmically determined end of the GI in the $\delta^{18}O$ record.
i Difference between visually and algorithmically determined duration of the GI in the $\delta^{18}O$ record.
j Start of the GI in the $\delta^{18}O$ record, published by Rasmussen et al. (2014).
k End of the GI in the $\delta^{18}O$ record, published by Rasmussen et al. (2014).
l Duration of the GI in the $\delta^{18}O$ record, published by Rasmussen et al. (2014).
m Difference in duration between the visually determined one and that published by Rasmussen et al. (2014).
n Difference in duration between the algorithmically determined one and that published by Rasmussen et al. (2014).
o Duration of the abrupt transition in the GI $\delta^{18}O$ record determined visually.
p Duration of the abrupt transition in the GI $\delta^{18}O$ record determined algorithmically.
q Difference between the visually and algorithmically determined duration of the abrupt transition in the GI $\delta^{18}O$ record.
aa Start of the GI initial abrupt transition in the dust record, visually determined on annual-resolution data and rounded to the nearest decade.
bb End of the GI in the dust record, visually determined on annual-resolution data and rounded to the nearest decade.
cc Duration of the GI in the dust record, visually determined on annual-resolution data and rounded to the nearest decade.
dd Start of the GI initial abrupt transition in the dust record, algorithmically determined on annual-resolution data and rounded to the nearest decade.
ee End of the GI in the dust record, algorithmically determined on annual-resolution data and rounded to the nearest decade.
ff Duration of the GI in the dust record, algorithmically determined on annual-resolution data and rounded to the nearest decade.
gg Difference between visually and algorithmically determined start of the GI initial abrupt transition in the dust record.
hh Difference between visually and algorithmically determined end of the GI in the dust record.
ii Difference between visually and algorithmically determined duration of the GI in the dust record.
jj Start of the GI in the dust record, published by Rasmussen et al. (2014).
kk End of the GI in the dust record, published by Rasmussen et al. (2014).
ll Duration of the GI in the dust record, published by Rasmussen et al. (2014).
mm Difference in dust GI duration between the visually determined one and that published by Rasmussen et al. (2014).
nn Difference in dust GI duration between the algorithmically determined one and that published by Rasmussen et al. (2014).
oo Duration of the abrupt transition in the GI dust record determined visually.
pp Duration of the abrupt transition in the GI dust record determined algorithmically.
qq Difference between the visually and algorithmically determined duration of the abrupt transition in the GI dust record.

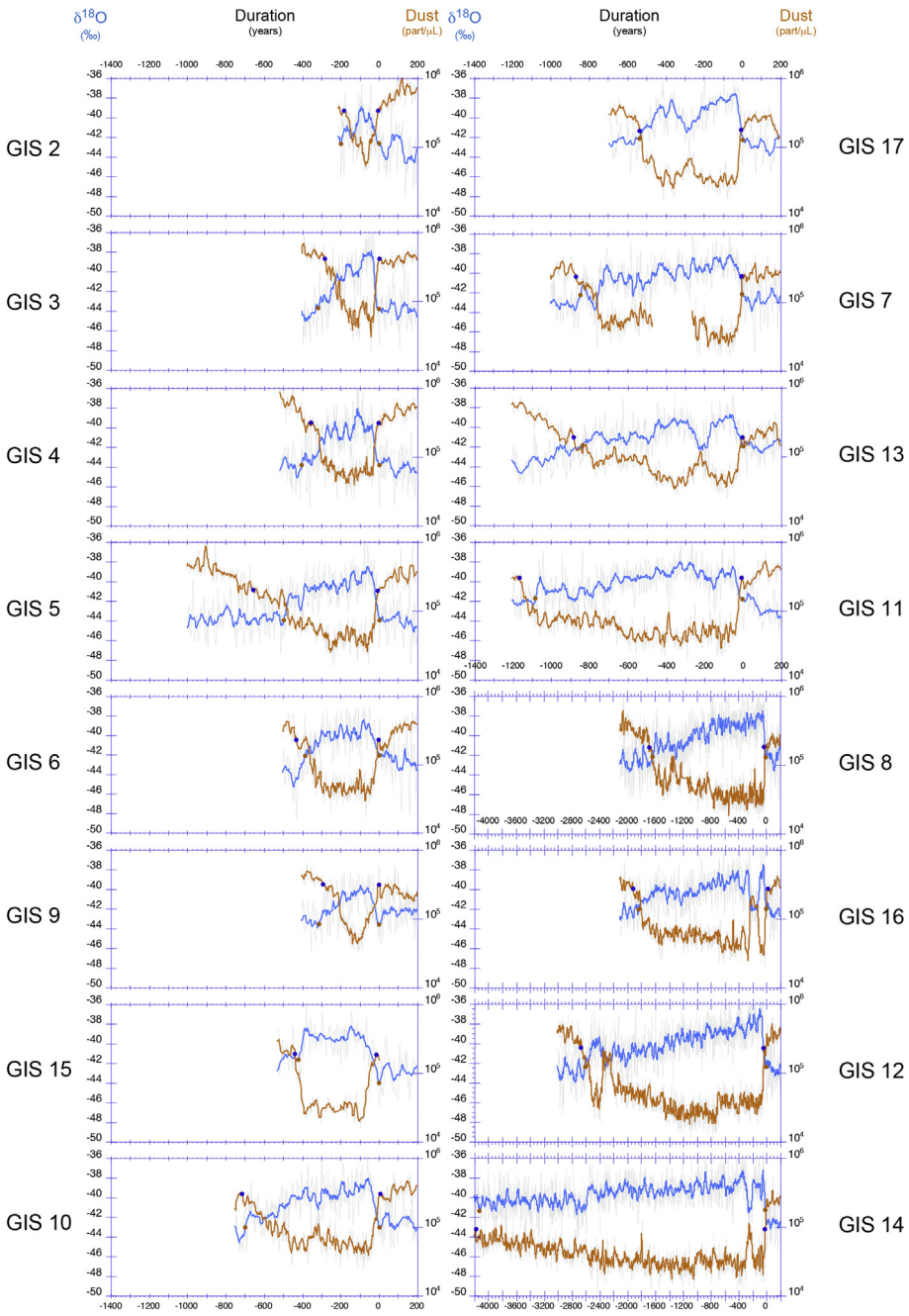

Fig. 5. Greenland interstadials 17 to 2 gathered in two groups depending of the duration. The first group gathers GI 2, 3, 4, 5, 6, 9, 15, 10, 17, 7, 13 and 11. The second group gathers GI 8, 16, 12 and 14, which show the longest duration. The start and the end of the event, as explained in Fig. 3, are indicated the same way, blue dots for the dust concentration and red dots for the $\delta^{18}O$. GI 15, 16 and 17 (in italic) are not clearly identified in Nussloch loess sequence. (For interpretation of the references to colour in this figure legend, the reader is referred to the web version of this article.)

already at the precursor event, based on considering the magnitude of the parameter variations, which are similar in the $\delta^{18}O$ while the first abrupt changes in the dust record starts from much higher concentration than the second one, indicating some already prevailing climate dynamics.

3.1.2. GI end

The **GI end,** as we choose to visually define it here (i.e., the date of return to the value at the beginning of the initial abrupt change), is less difficult to pinpoint than using the Wolff et al. (2010) criterion (i.e., the end of the decrease towards stadial values). It corresponds to a return to the previous stadial conditions determined by both $\delta^{18}O$ and dust concentration (Fig. 3).

3.1.3. GI onsets

The GI onsets were determined by our algorithm in two slightly different ways for comparison: Two different percentile values were computed for the pre-transition period that was chosen for the threshold to determine when the abrupt transition started: the 50^{th} percentile as stated in the third step of the algorithm above, and, for comparison, the 75th percentile. For the 75th percentile (higher threshold), the transitions tend to start later than for the

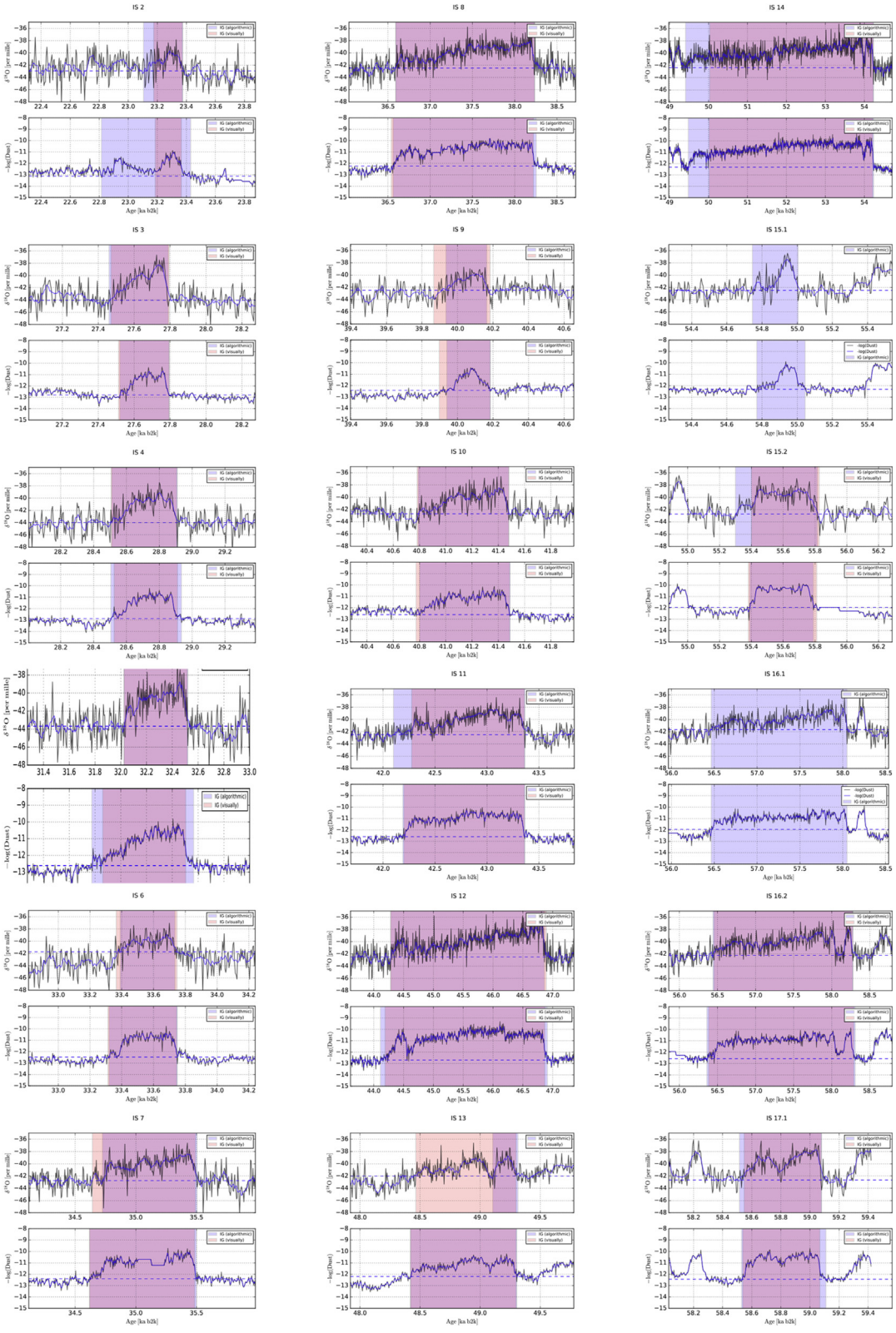

Fig. 6. Greenland interstadials 17 to 2 as expressed through variations in the $\delta^{18}O$ (top panel) and dust concentration (low panel) records. Identification of the start and end dates of the interstadials as determined visually (pink shaded) and algorithmically (blue shaded). (For interpretation of the references to colour in this figure legend, the reader is referred to the web version of this article.)

50th percentile (lower threshold). The onset times computed with the lower threshold (50^{th} percentile) are more inline with the visual determination for the NGRIP $\delta^{18}O$ data, showing only minimal differences. Nevertheless, applying this lower threshold leads to earlier onset dates for the dust record (see Table 2).

The algorithmic determination of the transition onset dates

allows to identify events 15.1 and 16.1 (Rasmussen et al., 2014), which were not identified during the original, visual determination (Dansgaard et al., 1993; Johnsen et al., 2001). A comparison between the visually and algorithmically determined start and end dates of the GIs suggests that they can be different in the $\delta^{18}O$ and dust concentration for a single event, in contradiction with the general interpretation by Rasmussen et al. (2014), who report similar dates of start and end dates of the identified GIs for both $\delta^{18}O$ and dust concentration (Table 2).

3.2. NGRIP GI visually determined duration (Fig. 5)

Considering the degree of subjectivity associated with the layer counting method, we only estimate the **GI duration**, i.e. the time difference between GI start and end dates (Fig. 3) in the dust and $\delta^{18}O$ records, to the nearest century (Table 1, columns *f,g*) or to the nearest decade, depending on the applied method (Table 2, columns c,f,i,cc,ff,ii). Such degree of precision is sufficient for our main purpose, which is to estimate the time span available for the development of different paleosol types in Europe during the last climate cycle.

The GI durations from the $\delta^{18}O$ data are compared to the values determined by Wolff et al. (2010) on the basis of the same record (Table 1, column *h*). For 7 out of the 11 GIs (from GI 12 to 2) they have estimated, we obtain the same duration. The other 4 GI durations are longer, by one century for GI 11, 4 and 2, and by two centuries in the case of GI 7.

A comparison between the visually and algorithmically determined start and end dates of the GIs first suggests that these dates are different for the two observables ($\delta^{18}O$ and dust) in numerous interstadials (Fig. 6) (Table 2 columns a, b, d, e, aa, bb, dd, ee). This is in contradiction with the general interpretation of Rasmussen et al. (2014), who report similar dates of start and end of the identified GI in both $\delta^{18}O$ and dust records. Let us consider the duration difference (rounded to the nearest century) between the two methods we applied (Table 2, column i). Concerning the $\delta^{18}O$ record, 9 out of 16 GI have similar durations (GI 3, 4, 5, 6, 8, 10, 12, 16.2 and 17.1) in both methods (visual versus algorithmic). In contrast, GI 7 and 9 are longer by one century and GI 13 by 6 centuries, while GI 2 and 15.2 are shorter by one century, GI 11 by 2 and GI 14 by 6 centuries when determined visually. Concerning dust, 10 out of 16 GIs have similar duration with both methods (GI 3, 4, 5, 6, 7, 8, 11, 12, 16.2 and 17.1) while GI 9, 10, 13 and 15.2 are longer by one century and GI 2 and 14 are shorter by 4 and 5 centuries respectively when determined visually (Table 2, column ii).

If we compare our duration estimates (obtained from both methods) to those released by Rasmussen et al. (2014), we also get different results (Table 2, columns m, n, mm, nn): First, the average duration of $\delta^{18}O$ GIs varies from 1050 ± 1070 yr, 1050 ± 1170 yr to 930 ± 1130 yr when analyzed visually, algorithmically and published by Rasmussen et al. (2014) (Table 2, columns c,f,i). Second, minimum and maximum duration of the GIs vary between 200 and 4200 yr, 200–4900 yr and 100–4600 yr, respectively. 8 out of 16 GI are visually of the same duration as reported by Rasmusen et al. (2014), 6 are longer and 2 shorter. 7 out of 18 GIs are algorithmically of similar duration than in Rasmussen et al. (2014), 10 are longer and 1 is shorter. Second, the average duration of dust GI varies from 1080 ± 1080 yr, 1080 ± 30 yr, to 930 ± 1130 yr (Table 2, columns cc, ff, ii) respectively for the record analyzed visually, algorithmically or as published in Rasmussen et al. (2014). 10 out of 18 GI are algorithmically of the same duration as Rasmussen et al. (2014), 5 are longer and 3 are shorter.

Interestingly, the NGRIP high-resolution data changed our understanding of the abruptness of dust and $\delta^{18}O$ variations. In our previous studies (Rousseau et al., 2007b, 2011) we have used the GRIP Ca^{2+} (representing dust) record for correlation with the loess sequences, because at its 50-year temporal resolution the stadial-interstadial transitions appeared much sharper than in the $\delta^{18}O$. This does not seem to be the case for the NGRIP high-resolution dataset (Fig. 5; Table 2).

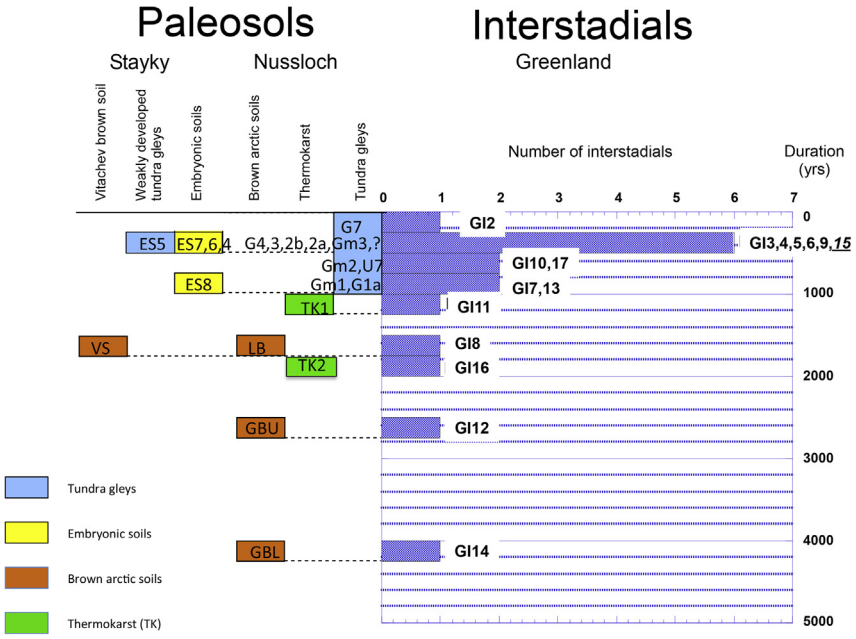

Fig. 7. Paleosol units identified in the European loess series along a 50°N longitudinal transect and their related GI (see the correlation between the identified paleosols and GI in Fig. 2). The maximum duration of the paleosol formation, among other parameters, infers the maturation of the pedogenesis and corresponds to the duration of the GI according to the methodologies applied in this study. The blue histogram on the right hand side shows the number of interstadials/paleosols per unit of duration. The colored boxes identified the different pedogenic units identified in the sequence including two thermokarst events. The labels of the paleosol units refer to those used in Fig. 2. (For interpretation of the references to colour in this figure legend, the reader is referred to the web version of this article.)

Table 3
Duration of GI 17 to 2 transition time in the NGRIP dust and $\delta^{18}O$ records, on the GICC05 timescale (in bold when the dust-derived value differs from the $\delta^{18}O$ one for a given GI), same references as in Table 1.

GIS	NGRIP records		Fleitman et al. (2009)		
	a) in the dust record (yr) this study	b) in the $\delta^{18}O$ ice record (yr) this study	c) Speleothem transition (yr)	d) 1ó (yr)	e) Difference (c) − (b) (yr)
2	60	50	n.d.	n.d.	n.d.
3	40	40	20	**17**	**20**
4	30	30	40	31	−10
5	60	60	40	48	20
6	70	80	120	55	−40
7	70	60	40	54	20
8	40	50	80	42	−30
9	110	60	20	**32**	**40**
10	60	60	40	34	20
11	40	50	160	**72**	**−110**
12	70	90	60	44	30
13	60	50	n.d.	n.d.	n.d.
14	50	50	n.d.	n.d.	n.d.
15	80	80	n.d.	n.d.	n.d.
16	40	40	n.d.	n.d.	n.d.
17	40	40	n.d.	n.d.	n.d.
Average transition (yr)	57.5	55.6			
1ó (yr)	20.2	16.3			

[a)] GI transition time in the dust record, visually determined on annual-resolution data and rounded to the nearest decade.
[b)] Same as [a)] for the $\delta^{18}O$ record.
c) GI transition estimated to the nearest decade on speleothem record by Fleitman et al. (2009).
d) Estimated error on the GI transition time from speleothem record by Fleitman et al. (2009).
e) Difference between the GI transition time estimated here (b) and the Fleitman et al. (2009). values [(c)].

Considering the determined correlations between the Nussloch paleosol series and the NGRIP GIs (Fig. 2), our study also indicates that the GIs can be grouped into two categories for the considered time interval 60 ka to 23 ka b2K: the interstadials lasting roughly between 200 and 1200 years and those lasting between 1800 to more than 4000 years (Fig. 7). This interpretation is in line with Yaalon's (1971) interpretation of his two categories of soil diagnostic features and horizons, the rapidly adjusting features which are reversible and last less than 10^2–10^3 years on the one hand, and the slowly adjusting, irreversible features, in which influx exceeds efflux, and which last more than 10^3–10^4 years. Fig. 5 shows the visually determined GI events 17 to 2 in the NGRIP dust and $\delta^{18}O$ records, on a relative time scale starting at the beginning of the abrupt change. For each GI, the estimated start and end are pinpointed on both $\delta^{18}O$ and dust records. Fig. 6 shows NGRIP $\delta^{18}O$ and dust GI events 17.1 to 2 on the NGRIP time scale with visual (pink) and algorithmic (blue) GI estimates. Considering the counting errors associated with the NGRIP data and the protocol used in our estimation of the event limits, and because of the aim of our study, the two observables ($\delta^{18}O$ and dust) can be interpreted as starting simultaneously within a single decade even if recent high-resolution studies seem to show some differences that cannot be addressed in this paper.

Considering the duration of the GI deduced from the dust and the $\delta^{18}O$ records (Tables 2 and 3), although the two main paleosol categories are identified, one could question if any particular difference happened in the abruptness of the transition between stadial and interstadial conditions during the considered intervals (Table 3, columns *a, b*). In our study, the transitions in both dust and $\delta^{18}O$ records occurred in roughly the same time range with the visual method; the transition duration varies between a minimum of 30 years and a maximum of 90 years, an exceptional longer value of 110 years being noticed for the transition to GI 9 in the dust record. With the algorithmic method, the transition varies between a minimum of 30 years and a maximum of 90 years, with an exceptional maximum of 120 years for GI 5 dust and a minimum of 10 years for GI 9 $\delta^{18}O$ (Table 2). If we compare with the transition values indicated by Fleitmann et al. (2009) from a Turkish speleothem covering GI 12 to 3, the difference with our observations falls within the error range proposed for the studied concretion varying between 72 and 17 years. Following our protocol, the transition in the $\delta^{18}O$ and in the dust concentration records in Greenland lasts the same time for eight GI, while the dust transition is longer by about 10 years for all remaining cases except GI 9. The $\delta^{18}O$ transition is longer by 10–20 years in the range of the errors provided by Fleitmann et al. (2009) (Table 3, column *c*).

Our study indicates similar transitions, rapid and abrupt during glacial time, as those obtained for the Late Glacial interval for the same parameters (Steffensen et al., 2008). The average transition duration is of 55.4 ± 16.1 yr or 36.4 ± 13.4 yr for the $\delta^{18}O$ and 56.8 ± 19.6 yr or 60.0 ± 21.2 yr for the dust concentration, determined using the visual and algorithmic methods, respectively (Table 2, columns o,p, oo, pp). This can still be considered as brutal, even if less sharp as the deuterium excess changes noticed for the Late Glacial interval (Steffensen et al., 2008). A recent reconstruction of the NGRIP temperature variations reveals temperature increase during the Dansgaard-Oeschger (GI) warming on average of about 11.8 °C during our determined time transition (Kindler et al., 2013). This corresponds to an average 0.21 °C per year temperature increase on top of the Greenland ice-sheet, a substantial one, even if at lower European latitudes where the paleosols developed, the magnitude of the warming should have been much lower.

4. Low atmospheric dust load intervals in Greenland ice and pedogenesis in Europe

When Greenland experienced abrupt warming and dust concentration decreased, dust emission at mid-latitudes also strongly decreased in Europe, sources almost completely ceased to emit, allowing paleosols to develop. Dust emission should have persisted

in desert areas but probably at a reduced rate in comparison to stadial conditions, at least in northern Chinese deserts, which are the source of the dust deposited in the Greenland ice (Svensson et al., 2000). This still permitted particle transport towards the western Pacific and Greenland, similarly to present time, since the dust concentration in the ice-cores never completely vanished. On the contrary, the paleosol development during GIs over European mid-latitudes occurred directly in a landscape covered by eolian material as every sequence clearly indicates. This was marked by increased biological activity such as the development of adapted mollusk faunas, compared to loess stadial intervals, and increased earthworm activity: burrowing, spheroid production in large quantities, is characterizing warmer environments (Moine et al., 2005, 2008; Antoine et al., 2009; Prud'homme et al., 2016). Moister conditions (Rousseau et al., 1990; Rousseau, 2001; Hatté et al., 2013; Moine, 2008, 2014) also prevailed due to increased precipitation (Sima et al., 2013; Rousseau et al., 2014) and corresponded to a direct response by the continental environments to changes affecting the marine circulation, especially in the Northern Atlantic. This was demonstrated at lower latitudes than our 50°N band, as this affected the vegetation inland the Iberian Peninsula and in Italy (Allen et al., 1999; Sanchez-Goni et al., 2000; Nebout et al., 2009). However, the terrestrial responses, i.e. vegetation, showed a slight delay to the change in the North Atlantic sea surface temperatures contrary to Greenland $\delta^{18}O$, which seem to show a more synchronous reaction with marine changes. The vegetation changes also occurred at northern latitudes in the loess corridor as recorded by the $\delta^{13}C$ from the organic matter originating from grass that is preserved in the sediments, the presence of which is marked by the preserved grass root casts in the loess units (Hatté et al., 2013) and the high concentration of cool and moist loving terrestrial mollusks (Moine et al., 2008). Annual precipitation estimates established from the inverse modeling of the $\delta^{13}C$ indicate higher values during the interstadials than during stadials (Hatté and Guiot, 2005). Strong water stress also occurred within the vegetation during stadials, mostly in Eastern Europe as observed in Serbia and the Czech Republic through the record of C4 plants from $\delta^{13}C$ analyses of the organic matter preserved in the sediment (Hatté et al., 2013).

Considering the abruptness of the warmings and the maximum duration of the interstadials, warmer, moister, more stable environmental conditions with more biological activity were therefore, at least in Europe, extremely favorable for different types of soil development corresponding to a complete restructuring of the environment and of the local ecosystems. The modeling experiments by Sima et al. (2009, 2013) indicate that the dust emission was extremely reduced during GIs. This is probably due not only to increased precipitation over the dry source areas, but also to more developed vegetation, e.g. grass. More frequent floodings of the main river valleys or higher water levels have to be considered as well, as they represented common suppliers of coarse dust particles during the stadials (Rousseau et al., 2014), especially from late winter to early summer, the time interval simulated as most favorable for dust emission in Europe.

A pattern emerges therefore after ranking the different paleosols observed in Nussloch and Stayky, the two key reference sequences investigated along the 50°N transect, located at a distance of about 1800 km (Fig. 7). It reflects both the exposure of the studied sequences to the heat and moisture transported from the Atlantic Ocean, and the intensity of the soil development mainly as a function of temperature and time. The estimated time values for the whole pedogenesis are nevertheless maximal with the exact duration of soil development being probably much shorter especially for the gleys (Fig. 7). All identified gleyed horizons are of short maximum duration, never longer than 1000 years and varying down to about 200 years, the latter corresponding to less expressed units in the stratigraphy. On the contrary, the brown arctic paleosols clearly indicate a maximum duration varying from a minimum of 1600 years for the youngest (GI 8) to about 4200 years for GI 14, so far also the longest of the considered 60 ka −23 ka interval (Table 1, columns *f, g*; Table 2, columns c,f,cc,ff).

Knowing i) the abruptness of the change in environmental conditions between full stadials and interstadials, and ii) the maximum duration of the soil development concerned, the question of the end of a particular episode and the start of the eolian deposition in Europe still remains. In the observed stratigraphies, the upper limit of a paleosol is always particularly well-differentiated from the overlying loess unit. For the time concerned, this upper limit (the former surface) usually corresponds to the start of the soil development. However, this upper limit of the paleosol represents i) the older abrupt transition event and going downward the soil moves the stratigraphy to younger ages, and ii) the youngest boundary of the overlying new eolian interval. Comparing our continental records with the Greenland data as we do in the present study, it would be easier and simpler to consider the time during which the dust deposition is lowest until the first event encountered in the record (Rousseau et al., 2007b), corresponding to some important change occurring in the records. However, considering now the high-resolution data from NGRIP, such strategy is no more conceivable because of the complexity of the records, which would lead to an overinterpretation of the available data. This is thus a more complicated issue that cannot be addressed with the present continental material and tools available for this study. Therefore, we prefer adopting a conservative position by proposing that the dust eolian deposition resumed in Europe somehow at the dates considered for the maximum duration of the interstadials.

5. Conclusions

The high resolution $\delta^{18}O$ and dust concentration records obtained from the NGRIP ice-core that was drilled at the top of the Greenland ice-sheet reveal important patterns of abrupt climatic changes referred to as Dansgaard-Oeschger events. They are related to environmental and climatic changes that impacted Europe and are mainly preserved in the loess sequences located on a longitudinal transect at 50°N. The perfect correspondence between the Greenland interstadials and the paleosols succession described from the studied loess sequences also at high resolution allows to determine two main categories in the identified European soil horizons, with estimation of a maximum soil development which still remains indicative and corresponds to a maximum duration of development. Indeed, although tundra gleys and oxidized horizons correspond to a maximum development duration varying between 1000 and 200 years along the transect, the better developed brown arctic soils correspond to intervals of maximum soil formation varying between 4200 and 1600 years when visually determined and 4800 and 1700 years when algorithmically determined. The transition phase between stadial conditions to interstadial ones, corresponding to a maximum of warming and of decrease in dust concentration, occurred in Greenland ice within almost identical time intervals: 55.4 ± 16.1 (visual) versus 36.4 ± 13.4 (algorithmic) years for the $\delta^{18}O$ and 56.8 ± 19.6 (visual) versus 60.0 ± 21.2 (algorithmic) years for the dust. This remains abrupt in mid-latitude Europe at an ecosystem level and is marked by a sharp boundary in the field between the considered paleosol and the overlying loess eolian unit. The temperature changes reconstructed from measurements of $\delta^{15}N$ in the same ice-core indicates that on average, the warming which lasted about 56 years was of 11.8 °C over Greenland (Kindler et al., 2013). This is considerable but fits with the observed changes in the stratigraphy, even if at mid-

latitude Europe the warmings might have been less intense than over Greenland. This abruptness, which is similar to the ones described for the Late Glacial of the same record, still permits to interpret that the paleosols developed almost instantaneously every time as a response to drastic climate changes, especially in temperature and precipitation favoring biological activity of variable intensity. The dust deposition over Europe almost ceased due to these very rapid changes allowing terrestrial ecosystems to evolve very rapidly from the parental eolian material with scarce vegetation to more vegetated ones in response to the new climate conditions. An estimate of when the eolian deposition resumed in Europe is not easy to establish; probably during the return towards stadial conditions but there is no argument yet to strongly support such assertion. Therefore we remain considering the restart of the eolian deposition, by convention, at the end of the interstadial.

Acknowledgements

This work was supported by the French ANR through grant ANR-08-BLAN-0227 to PI DDR, and completed during a Visiting Professorship to Columbia University by DDR supported by the Alliance program. N.B. acknowledges funding by the Alexander von Humboldt Foundation and the German Federal Ministry for Education and Research. CNRS-INSU rejected a support request to DDR for the completion this study because of the lack of innovation and interest but hopefuly thoughts remain free. We dedicate this paper to Sigfus Johnsen, who unfortunately left us too early but was strongly supportive of this study. He was a great colleague and scientist who always supported these ice-core-continental comparisons. This is LDEO 8115 contribution and IPGP 3850 contribution.

NGRIP is directed and organized by the Ice and Climate research group, Niels Bohr Institute, University of Copenhagen. It is supported by funding agencies in Denmark (FNU), Belgium (FNRS-CFB), France (IPEV and INSU,CNRS), Germany (AWI), Iceland (RANNIS), Japan (MEXT), Sweden (SPRS), Switzerland (SNF) and the USA (NSF, Office of Polar Programs).

The used data sets are available at" www.icecores.dk"

Appendix A. Supplementary data

Supplementary data related to this article can be found at http://dx.doi.org/10.1016/j.quascirev.2017.05.020.

References

Allen, J.R.M., Brandt, U., Brauer, A., Hubberten, H.W., Huntley, B., Keller, J., Kraml, M., Mackensen, A., Mingram, J., Negendank, J.F.W., Nowaczyk, N.R., Oberhansli, H., Watts, W.A., Wulf, S., Zolitschka, B., 1999. Rapid environmental changes in southern Europe during the last glacial period. Nature 400, 740–743.

Andersen, K.K., Svensson, A., Johnsen, S.J., Rasmussen, S.O., Bigler, M., Rothlisberger, R., Ruth, U., Siggaard-Andersen, M.L., Steffensen, J.P., Dahl-Jensen, D., Vinther, B.M., Clausen, H.B., 2006. The Greenland Ice Core Chronology 2005, 15-42 ka. Part 1: constructing the time scale. Quat. Sci. Rev. 25, 3246–3257.

Antoine, P., Lozouet, N.L., Chausse, C., Lautridou, J.-P., Pastre, J.-F., Auguste, P., Bahain, J.-J., Falgueres, C., Galehb, B., 2007. Pleistocene fluvial terraces from northern France (Seine, Yonne, Somme): synthesis, and new results from interglacial deposits. Quat. Sci. Rev. 26, 2701–2723.

Antoine, P., Rousseau, D.D., Degeai, J.P., Moine, O., Lagroix, F., kreutzer, S., Fuchs, M., Hatté, C., Gauthier, C., Svoboda, J., Lisa, L., 2013. High-resolution record of the environmental response to climatic variations during the Last Interglacial-Glacial cycle in Central Europe: the loess-palaeosol sequence of Dolní Věstonice (Czech Republic). Quat. Sci. Rev. 67, 17–38.

Antoine, P., Rousseau, D.D., Fuchs, M., Hatte, C., Gauthier, C., Markovic, S.B., Jovanovic, M., Gaudenyi, T., Moine, O., Rossignol, J., 2009. High-resolution record of the last climatic cycle in the southern Carpathian Basin (Surduk, Vojvodina, Serbia). Quat. Int. 198, 19–36.

Antoine, P., Rousseau, D.D., Zöller, L., Lang, A., Munaut, A.V., Hatté, C., Fontugne, M., 2001. High-resolution record of the last interglacial-glacial cycle in the loess palaeosol sequences of Nussloch (Rhine Valley-Germany). Quat. Int. 76/77, 211–229.

Antoine, P., Coutard, S., Guerin, G., Deschodt, L., Goval, E., Locht, J.L., Paris, C., 2016. Upper Pleistocene loess-palaeosol records from Northern France in the European context: environmental background and dating of the Middle Palaeolithic. Quat. Int. 411, 4–24. http://dx.doi.org/10.1016/j.quaint.2015.11.036.

Bibus, E., Frechen, M., Kösel, M., Rähle, W., 2007. Das jungpleistozäne Lössprofil von Nussloch (SW-Wand) im Aufschluss der Heidelberger Zement AG. Eiszeitalt. Ggw. 56, 227–255.

Birkeland, P.W., 1984. Soils and Geomorphology. Oxford University Press, New-York-Oxford.

Boch, R., Cheng, H., Spotl, C., Edwards, R.L., Wang, X., Hauselmann, P., 2011. NALPS: a precisely dated European climate record 120-60 ka. Clim. Past 7, 1247–1259.

Bond, G., Heinrich, H., Broecker, W., Labeyrie, L., McManus, J., Andrews, J., Huon, S., Jantschik, R., Clasen, S., Simet, C., Tedesco, K., Klas, M., Bonani, G., Ivy, S., 1992. Evidence for massive discharges of icebergs into the North Atlantic Ocean during the last glacial period. Nature 360, 245–249.

Byrkjedal, O., Kvamsto, N., Meland, M., Jansen, E., 2006. Sensitivity of last glacial maximum climate to sea ice conditions in the Nordic Seas. Clim. Dyn. 26, 473–487.

Capron, E., Landais, A., Chappellaz, J., Schilt, A., Buiron, D., Dahl-Jensen, D., Johnsen, S.J., Jouzel, J., Lemieux-Dudon, B., Loulergue, L., Leuenberger, M., Masson-Delmotte, V., Meyer, H., Oerter, H., Stenni, B., 2010. Millennial and sub-millennial scale climatic variations recorded in polar ice cores over the last glacial period. Clim. Past 6, 345–365.

Dansgaard, W., Johnsen, S.J., Clausen, H.B., Dahi-Jensen, D., Gundestrup, N.S., Hammer, C.U., Hvidberg, C.S., Steffensen, J.P., Sveinbjöprnsdottir, A.E., Jouzel, J., Bond, G., 1993. Evidence for general instability of past climate from a 250-kyr ice-core record. Nature 364, 218–220.

Fischer, H., Siggaard-Andersen, M.L., Ruth, U., Rothlisberger, R., Wolff, E., 2007. Glacial/interglacial changes in mineral dust and sea-salt records in polar ice cores: sources, transport, and deposition. Rev. Geophys. 45.

Fleitmann, D., Cheng, H., Badertscher, S., Edwards, R.L., Mudelsee, M., Goektuerk, O.M., Fankhauser, A., Pickering, R., Raible, C.C., Matter, A., Kramers, J., Tuysuz, O., 2009. Timing and climatic impact of Greenland interstadials recorded in stalagmites from northern Turkey. Geophys. Res. Lett. 36.

Fletcher, W.J., Goni, M.F.S., Allen, J.R.M., Cheddadi, R., Combourieu-Nebout, N., Huntley, B., Lawson, I., Londeix, L., Magri, D., Margari, V., Mueller, U.C., Naughton, F., Novenko, E., Roucoux, K., Tzedakis, P.C., 2010. Millennial-scale variability during the last glacial in vegetation records from Europe. Quat. Sci. Rev. 29, 2839–2864.

Genty, D., Blamart, D., Ouahdi, R., Gilmour, M., Baker, A., Jouzel, J., Van-Exter, S., 2003. Precise dating of Dansgaard-Oeschger climate oscillations in western Europe from stalagmite data. Nature 421, 833–837.

Gkinis, V., Simonsen, S.B., Buchardt, S.L., White, J.W.C., Vinther, B.M., 2014. Water isotope diffusion rates from the NorthGRIP ice core for the last 16,000 years – Glaciological and paleoclimatic implications. Earth Planet. Sci. Lett. 405, 132–141. http://dx.doi.org/10.1016/j.epsl.2014.08.022.

Hatté, C., Antoine, P., Fontugne, M., Rousseau, D.D., Tisnérat-Laborde, N., Zöller, L., 1999. New chronology and organic matter $\delta^{13}C$ paleoclimatic significance of Nussloch loess sequence (Rhine Valley, Germany). Quat. Int. 62, 85–91.

Hatté, C., Gauthier, C., Rousseau, D.D., Antoine, P., Fuchs, M., Lagroix, F., Markovic, S.B., Moine, O., Sima, A., 2013. Excursions to C4 vegetation recorded in the upper Pleistocene loess of surduk (Northern Serbia): an organic isotope geochemistry study. Clim. Past 9, 1001–1014.

Hatté, C., Guiot, J., 2005. Paleoprecipitation reconstruction by inverse modelling using the isotopic signal of loess organic matter: application to the Nussloch loess sequence (Rhine Valley, Germany). Clim. Dyn. 25, 315–327.

Johnsen, S.J., Dahl-Jensen, D., Gundestrup, N., Steffensen, J.P., Clausen, H.B., Miller, H., Masson-Delmotte, V., Sveinbjörnsdottir, A.E., White, J., 2001. Oxygen isotope and palaeotemperature records from six Greenland ice-core stations: camp Century, Dye-3, GRIP, GISP2, Renland and NorthGRIP. J. Quat. Sci. 16, 299–307.

Juvigné, E., 1985. The use of heavy mineral suites for lœss stratigraphy. Geol. Mijnb. 64, 333–336.

Kadereit, A., Kind, C.-J., Wagner, G.A., 2013. The chronological position of the Lohne Soil in the Nussloch loess section - re-evaluation for a European loess-marker horizon. Quat. Sci. Rev. 59, 67–86.

Kindler, P., Guillevic, M., Baumgartner, M., Schwander, J., Landais, A., Leuenberger, M., 2013. NGRIP temperature reconstruction from 10 to 120 kyr b2K. Clim. Past 9, 4099–4143.

Kutzbach, J.E., Guetter, P.J., 1986. The influence of changing orbital parameters and surface boundary-conditions on climate simulations for the past 18000 years. J. Atmos. Sci. 43, 1726–1759.

Lang, A., Hatté, C., Rousseau, D.D., Antoine, P., Fontugne, M., Zöller, L., Hambach, U., 2003. High-resolution chronologies for loess: comparing AMS^{14}C and optical dating results. Quat. Sci. Rev. 22, 953–959.

Lautridou, J.P., 1985. Le cycle périglaciaire Pléistocène en Europe du Nord-Ouest et plus particulièrement en Normandie. Centre Géomorphologie Caen. Université Caen, Caen, p. 908.

Lautridou, J.P., Auffret, J.P., Baltzer, A., Clet, M., Lecolle, F., Lefebvre, D., Lericolais, G., Roblin-Jouve, A., Balescu, S., Carpentier, G., Descombes, J.C., Occhietti, S., Rousseau, D.D., 1999. The river Seine, the river Manche. Bull. De. La Soc. Geol. De. Fr. 170, 545–558.

Léger, M., 1990. Loess Landforms, 7/8. Quaternary International, pp. 53–61.

Masson-Delmotte, V., Jouzel, J., Landais, A., Stievenard, M., Johnsen, S.J., White, J.W.C., Werner, M., Sveinbjornsdottir, A., Fuhrer, K., 2005. GRIP

deuterium excess reveals rapid and orbital-scale changes in Greenland moisture origin. Science 309, 118–121.
Moine, O., 2008. West-European malacofauna from loess deposits of the Weichselian Upper Pleniglacial: compilation and preliminary analysis of the database. Quaternaire 19, 11–29.
Moine, O., 2014. Weichselian Upper Pleniglacial environmental variability in northwestern Europe reconstructed from terrestrial mollusc faunas and its relationship with the presence/absence of human settlements. Quat. Int. 337, 90–113.
Moine, O., Rousseau, D.D., Antoine, P., 2005. Terrestrial molluscan records of Weichselian Lower to Middle Pleniglacial climatic changes from the Nussloch loess series (Rhine Valley, Germany): the impact of local factors. Boreas 34, 363–380.
Moine, O., Rousseau, D.D., Antoine, P., 2008. The impact of Dansgaard-Oeschger cycles on the loessic environment and malacofauna of Nussloch (Germany) during the Upper Weichselian. Quat. Res. 70, 91–104.
Moine, O., Antoine, P., Hatté, C., Landais, A., Mathieu, J., Prud'Homme, C., Rousseau, D.D., 2017. The ^{14}C "earthworm Clock", 2017. A New Approach to Date the Impact of Last Glacial Climate Variability Recorded in West-European Loess. Proceedings of the National Academy of Sciences (in the press). http://dx.doi.org/10.1073/pnas.1614751114.
Müller, U.C., Pross, J., Bibus, E., 2003. Vegetation response to rapid climate change in Central Europe during the past 140,000 yr based on evidence from the Für-amoos pollen record. Quat. Res. 59, 235–245.
NGRIP members, 2004. High-resolution record of Northern Hemisphere climate extending into the last interglacial period. Nature 431, 147–151. http://dx.doi.org/10.1038/nature02805.
Nebout, N.C., Peyron, O., Dormoy, I., Desprat, S., Beaudouin, C., Kotthoff, U., Marret, F., 2009. Rapid climatic variability in the west Mediterranean during the last 25 000 years from high resolution pollen data. Clim. Past 5, 503–521.
Pausata, F.S.R., Li, C., Wettstein, J.J., Kageyama, M., Nisancioglu, K.H., 2011. The key role of topography in altering North Atlantic atmospheric circulation during the last glacial period. Clim. Past 7, 1089–1101.
Pecsi, M., 1990. Loess is not just the accumulation of dust. Quat. Int. 7/8, 1–21.
Prud'homme, C., Lécuyer, C., Antoine, P., Moine, O., Hatté, C., Fourel, F., Martineau, F., Rousseau, D.-D., 2016. Palaeotemperature reconstruction during the Last Glacial from $\text{TM}^{18}O$ of earthworm calcite granules from Nussloch loess sequence. Ger. Earth Planet. Sci. Rev. 442, 13–20. http://dx.doi.org/10.1016/j.epsl.2016.02.045.
Prud'homme, C., 2017. Les granules de calcite de vers de terre, un support innovant pour la reconstitution du paleoclimat du Dernier Glaciaire en milieu loessique européen: Application à l'étude des interactions Homme-environnement au Paléolithique. PhD thesis. University Paris1-Panthéon Sorbonne, 211pp.
Pye, K., 1987. Aeolian Dust and Dust Deposits. Academic Press.
Pye, K., 1995. The nature, origin and accumulation of loess. Quat. Sci. Rev. 14, 653–657.
Rasmussen, S.O., Andersen, K.K., Svensson, A.M., Steffensen, J.P., Vinther, B.M., Clausen, H.B., Siggaard-Andersen, M.L., Johnsen, S.J., Larsen, L.B., Dahl-Jensen, D., Bigler, M., Rothlisberger, R., Fischer, H., Goto-Azuma, K., Hansson, M.E., Ruth, U., 2006. A new Greenland ice core chronology for the last glacial termination. J. Geophys. Research-Atmos. 111.
Rasmussen, S.O., Bigler, M., Blockley, S.P., Blunier, T., Buchardt, S.L., Clausen, H.B., Cvijanovic, I., Dahl-Jensen, D., Johnsen, S.J., Fischer, H., Gkinis, V., Guillevic, M., Hoek, W.Z., Lowe, J.J., Pedro, J.B., Popp, T., Seierstad, I.K., Steffensen, J.P., Svensson, A.M., Vallelonga, P., Vinther, B.M., Walker, M.J.C., Wheatley, J.J., Winstrup, M., 2014. A stratigraphic framework for abrupt climatic changes during the Last Glacial period based on three synchronized Greenland ice-core records: refining and extending the INTIMATE event stratigraphy. Quat. Sci. Rev. 106, 14–28.
Rousseau, D.-D., Chauvel, C., Sima, A., Hatte, C., Lagroix, F., Antoine, P., Balkanski, Y., Fuchs, M., Mellett, C., Kageyama, M., Ramstein, G., Lang, A., 2014. European glacial dust deposits: geochemical constraints on atmospheric dust cycle modeling. Geophys. Res. Lett. 41, 7666–7674.
Rousseau, D.D., 2001. Loess biostratigraphy: new advances and approaches in mollusk studies. Earth-Sci. Rev. 54, 157–171.
Rousseau, D.D., Antoine, P., Gerasimenko, N., Sima, A., Fuchs, M., Hatte, C., Moine, O., Zoeller, L., 2011. North Atlantic abrupt climatic events of the last glacial period recorded in Ukrainian loess deposits. Clim. Past 7, 221–234.
Rousseau, D.D., Antoine, P., Hatté, C., Lang, A., Zöller, L., Fontugne, M., Ben Othman, D., Luck, J.M., Moine, O., Labonne, M., Bentaleb, I., Jolly, D., 2002. Abrupt millennial climatic changes from Nussloch (Germany) upper Weichselian eolian records during the last Glaciation. Quat. Sci. Rev. 21, 1577–1582.
Rousseau, D.D., Derbyshire, E., Antoine, P., Hatté, C., 2007a. European loess records. In: Elias, S. (Ed.), Encyclopedia of Quaternary Science. Elsevier, Amsterdam, pp. 1440–1456.
Rousseau, D.D., Puisségur, J.J., Lautridou, J.P., 1990. Biogeography of the Pleistocene pleniglacial malacofaunas in Europe. Stratigraphic and climatic implications. Palaeogeography, palaeoclimatology. Palaeoecology 80, 7–23.
Rousseau, D.D., Sima, A., Antoine, P., Hatte, C., Lang, A., Zöller, L., 2007b. Link between European and North Atlantic Abrupt Climate Changes over the Last Glaciation. Geophysical Research Letters, vol. 34.
Rousseau, D.D., Zöller, L., Valet, J.P., 1998. Late Pleistocene climatic variations at Achenheim, France based on a magnetic susceptibility and TL chronology of loess. Quat. Res. 49, 255–263.
Ruth, U., Bigler, M., Rothlisberger, R., Siggaard-Andersen, M.-L., Kipfstuhl, S., Goto-Azuma, K., Hansson, M.E., Johnsen, S.J., Lu, H., Steffensen, J.P., 2007. Ice core evidence for a very tight link between North Atlantic and east Asian glacial climate. Geophys. Res. Lett. 34.
Ruth, U., Wagenbach, D., Bigler, M., Steffensen, J.P., Röthlisberger, R., Miller, H., 2002. High resolution microparticle at NGRIP: case studies of the calcium-dust relationship. Ann. Glaciol. 35, 209–216.
Ruth, U., Wagenbach, D., Steffensen, J.P., Bigler, M., 2003. Continuous record of microparticle concentration and size distribution in the central Greenland NGRIP ice core during the last glacial period. J. Geophys. Res. 108, 4098, 4010.1029/2002JD002376.
Sanchez-Goni, M.F., Cacho, I., Turon, J.L., Guiot, J., Sierro, F.J., Peypouquet, J.P., Grimalt, J.O., Shackleton, N.J., 2002. Synchroneity between marine and terrestrial responses to millennial scale climatic variability during the last glacial period in the Mediterranean region. Clim. Dyn. 19, 95–105.
Sanchez-Goni, M.F., Turon, J.L., Eynaud, F., Gendreau, S., 2000. European climatic response to millennial-scale changes in the atmosphere-ocean system during the last glacial period. Quat. Res. 54, 394–403.
Sima, A., Kageyama, M., Rousseau, D.D., Ramstein, G., Balkanski, Y., Antoine, P., Hatté, C., 2013. Modeling dust emission response to North Atlantic millennial-scale climate variations from the perspective of East European MIS3 loess deposits. Clim. Past 9, 1385–1402.
Sima, A., Rousseau, D.D., Kageyama, M., Ramstein, G., Schulz, M., Balkanski, Y., Antoine, P., Dulac, F., Hatté, C., 2009. Imprint of North-Atlantic abrupt climate changes on western European loess deposits as viewed in a dust emission model. Quat. Sci. Rev. 28, 2851–2866.
Smalley, I., O'Hara-Dhand, K., Wint, J., Machalett, B., Jary, Z., Jefferson, I., 2009. Rivers and loess: the significance of long river transportation in the complex event-sequence approach to loess deposit formation. Quat. Int. 198, 7–18.
Steen-Larsen, H.C., Johnsen, S.J., Masson-Delmotte, V., Stenni, B., Risi, C., Sodemann, H., Balslev-Clausen, D., Blunier, T., Dahl-Jensen, D., Ellehoj, M.D., Falourd, S., Grindsted, A., Gkinis, V., Jouzel, J., Popp, T., Sheldon, S., Simonsen, S.B., Sjolte, J., Steffensen, J.P., Sperlich, P., Sveinbjornsdottir, A.E., Vinther, B.M., White, J.W.C., 2013. Continuous monitoring of summer surface water vapor isotopic composition above the Greenland Ice Sheet. Atmos. Chem. Phys. 13, 4815–4828.
Steffensen, J.P., Andersen, K.K., Bigler, M., Clausen, H.B., Dahl-Jensen, D., Fischer, H., Goto-Azuma, K., Hansson, M., Johnsen, S.J., Jouzel, J., Masson-Delmotte, V., Popp, T., Rasmussen, S.O., Rothlisberger, R., Ruth, U., Stauffer, B., Siggaard-Andersen, M.L., Sveinbjornsdottir, A.E., Svensson, A., White, J.W.C., 2008. High-resolution Greenland Ice Core data show abrupt climate change happens in few years. Science 321, 680–684.
Svensson, A., Andersen, K.K., Bigler, M., Clausen, H.B., Dahl-Jensen, D., Davies, S.M., Johnsen, S.J., Muscheler, R., Parrenin, F., Rasmussen, S.O., Roethlisberger, R., Seierstad, I., Steffensen, J.P., Vinther, B.M., 2008. A 60 000 year Greenland stratigraphic ice core chronology. Clim. Past 4, 47–57.
Svensson, A., Biscaye, P.E., Grousset, F.E., 2000. Characterization of late glacial continental dust in the Greenland Ice Core Project ice core. J. Geophys. Research-Atmos. 105, 4637–4656. http://dx.doi.org/10.1029/1999JD901093.
Taylor, S.N., Lagroix, F., Rousseau, D.-D., Antoine, P., 2014. Mineral magnetic characterization of the Upper Pleniglacial Nussloch loess sequence (Germany): an insight into local environmental processes. Geophys. J. Int. 199, 1463–1480.
Thomas, E.R., Wolff, E.W., Mulvaney, R., Johnsen, S.J., Steffensen, J.P., Arrowsmith, C., 2009. Anatomy of a dansgaard-oeschger warming transition: high-resolution analysis of the North Greenland ice core project ice core. J. Geophys. Research-Atmos. 114.
Tissoux, H., Valladas, H., Voinchet, P., Reyss, J.L., Mercier, N., Falgueres, C., Bahain, J.J., Zoeller, L., Antoine, P., 2010. OSL and ESR studies of Aeolian quartz from the Upper Pleistocene loess sequence of Nussloch (Germany). Quat. Geochronol. 5, 131–136.
Woillard, G., 1978. Grande pile peat bog : a continuous pollen record for the last 140,000 years. Quat. Res. 9, 1–21.
Wolff, E.W., Chappellaz, J., Blunier, T., Rasmussen, S.O., Svensson, A., 2010. Millennial-scale variability during the last glacial: the ice core record. Quat. Sci. Rev. 29, 2828–2838.
Yaalon, D.H., 1971. Soil Forming Processes in Space and Time. In: Yaalon, D.H. (Ed.), Paleopedology-Origin, Nature, and Dating of Paleosols. Israel University Press, Jerusalem, pp. 29–39.

Suppl. fig. 1

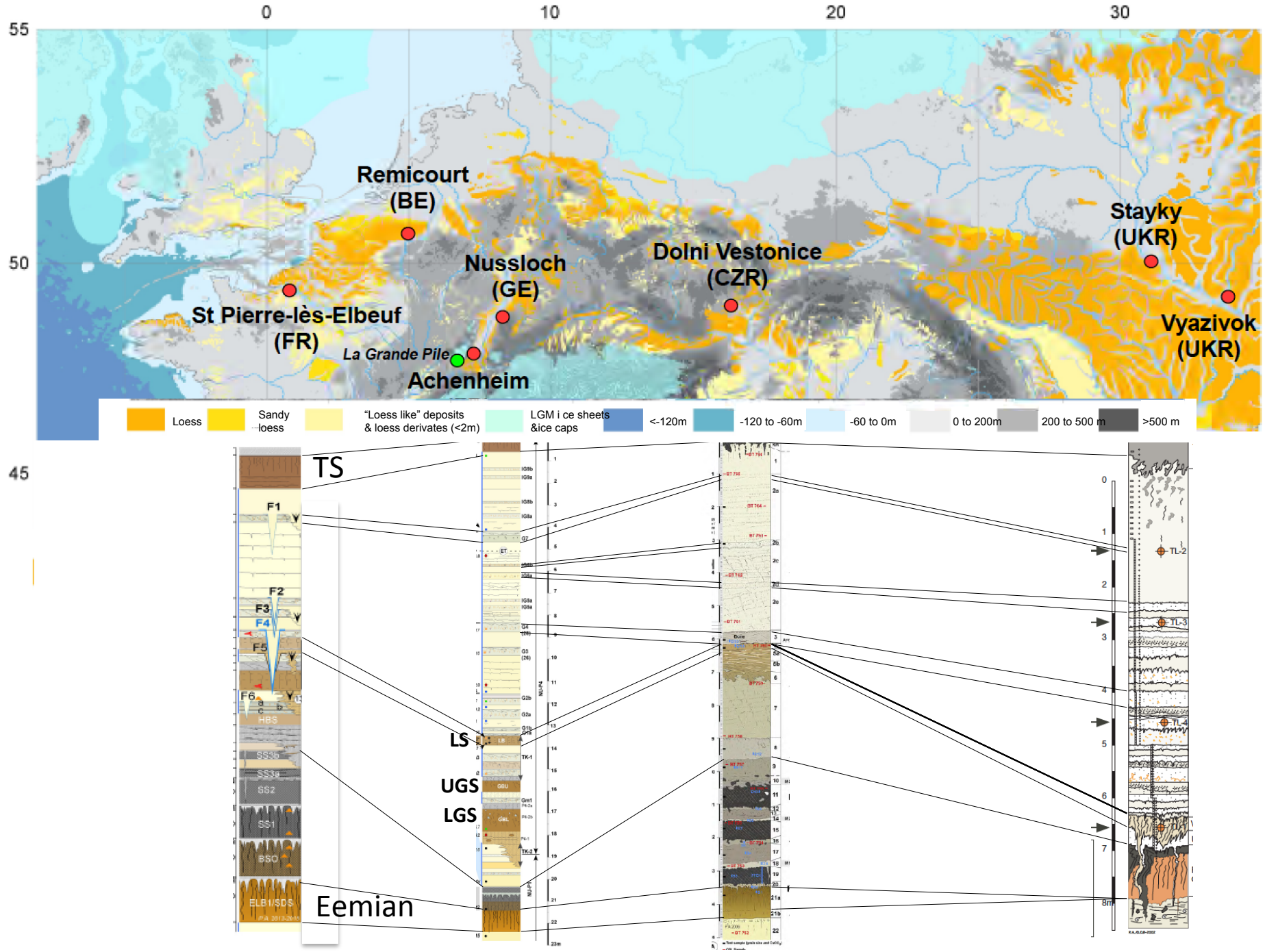
0
10
20
30
55
50
45
Remicourt
(BE)
Nussloch
(GE)
Dolni Vestonice
(CZR)
Stayky
(UKR)
Vyazivok
(UKR)
St Pierre-lès-Elbeuf
(FR)
La Grande Pile
Achenheim
Loess
Sandy loess
"Loess like" deposits & loess derivates (<2m)
LGM i ce sheets &ice caps
<-120m
-120 to -60m
-60 to 0m
0 to 200m
200 to 500 m
>500 m
TS
LS
UGS
LGS
Eemian
F1
F2
F3
F4
F5
F6
HBS
SS3
SS2
SS1
BSO
ELB I/SDS
TL-2
TL-3
TL-4

Suppl. fig. 2

Nussloch P4 pedostratigraphic units